Ultrafast Control of the Dimensionality of Exciton-Exciton Annihilation in Atomically Thin Black Phosphorus

Vivek Pareek, Julien Madéo, and Keshav M. Dani*
Femtosecond Spectroscopy Unit, Okinawa Institute of Science and Technology Graduate University, 1919-1 Tancha, Onna-son, Kunigami-gun 904-0495, Okinawa, Japan

(Received 10 June 2019; revised manuscript received 29 October 2019; accepted 2 January 2020; published 7 February 2020)

Using microtransient absorption spectroscopy, we show that the dynamical form of exciton-exciton annihilation in atomically thin black phosphorous can be made to switch between time varying 1D scattering and time-independent 2D scattering. At low carrier densities, anisotropy drives the 1D behavior, but as the photoexcitation density approaches the exciton saturation limit, the 2D nature of exciton-exciton scattering takes over. Furthermore, lowering the temperature provides a handle on the ultrafast timescale at which the 1D to 2D transition occurs. We understand our results quantitatively using a diffusion based model of exciton-exciton scattering.

DOI: 10.1103/PhysRevLett.124.057403

Exciton-exciton (X-X) annihilation is one of the key nonradiative recombination pathways in low-dimensional semiconductors impacting the performance of optoelectronic devices [1]. Interestingly, the nature of X-X annihilation exhibits strong dependence on the dimensionality of the system [2]. For example, in one-dimensional (1D) systems, the excitons are restricted to nearest neighbor interaction resulting in a time-dependent X-X annihilation rate [2–6]. Therefore, the exciton population can never reach steady state in 1D and shows a $1/\sqrt{t}$ decay with time, which is a suppression over the expected $1/t$ decay expected from the mean-field approximation [3,7]. In contrast, in two-dimensional (2D) systems, excitons can bypass nearest neighbors without interacting, which allows the exciton population to reach steady state rapidly, resulting in a time-independent rate of annihilation [8–10]. The excitonic population in 2D follows the $1/t$ decay predicted by mean-field theory [7]. These different forms of X-X annihilation observed in 1D and 2D systems have important technological and fundamental implications. For example, due to extreme exciton population depletion rates at early time delays, carbon nanotubes (CNTs) are unable to achieve high enough exciton densities to exhibit phenomena such as lasing [3] and Mott-insulator transition [11], whereas these phenomena have been observed in 2D transition metal dichalcogenides (TMDs) [12,13].

Among the various low-dimensional systems of current interest, a peculiar case is presented by excitons in few layer black phosphorus (BP). There the excitons show quasi-1D nature due to its unique puckered honeycomb lattice. The excitonic wave functions are quasi-1D, photoluminescence and optical absorption are strongly polarization dependent, and carrier diffusion highly favors the armchair direction [14–19]. Nonetheless, these quasi-1D excitons are present in a 2D lattice with the possibility of interaction along both armchair and zigzag crystal directions. This makes few layer BP an interesting platform to explore the dimensional form of excitonic interactions.

In this Letter, we show that the dimensional form of X-X annihilation in atomically thin BP can be made to switch between 1D and 2D by tuning the initial exciton density and sample temperature. In the low-density range of X-X annihilation, anisotropic diffusion dominates the scattering process, and we see 1D behavior similar to CNTs [3,4]. With increasing photoexcitation density, the increased probability of scattering along both zigzag and armchair directions smothers the effects of anisotropic diffusion, and we observe behavior similar to the 2D TMDs [8–10]. Finally, by decreasing the lattice temperature even at higher photoexcitation densities, we can recover 1D X-X annihilation phenomena.

For our study, we mechanically exfoliated bilayer (2L) BP of 3 μm size on fused silica substrate [Fig. 1(a)] in an inert environment and kept the sample under vacuum for all subsequent experiments to prevent degradation (see Supplemental Material for details [20]). PL measurements clearly indicate a bilayer structure with the expected emission at 1.13 eV or 1090 nm (see Supplemental Material, Fig. S1 [20]) [14,15]. We chose bilayer BP for our measurements due to its promise for existing optoelectronic technology [14,23,24], as well as due to experimental ease in fabrication and measurement. We expect qualitatively similar results for other few layers thick BP samples. To study the X-X annihilation process, we used a homebuilt microtransient absorption spectroscopy (μ-TAS) setup where we excite the sample just above the interband transition at 1.55 eV (800 nm) and probe over 1.24–1.03 eV (1000–1200 nm), thus covering the excitonic resonance [Fig. 1(b)]. We obtained 700 fs temporal resolution with submicron spatial resolution, allowing us to

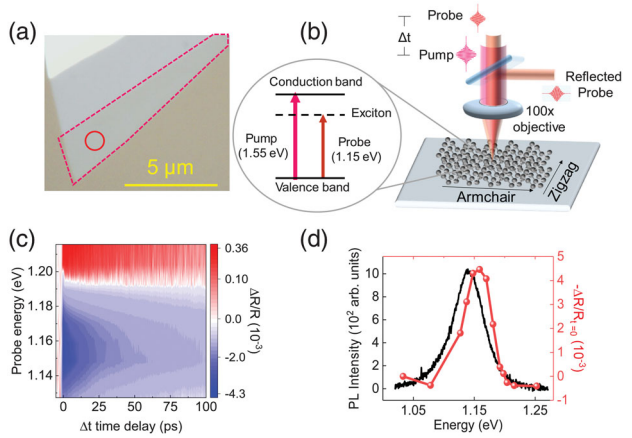

FIG. 1. Sample characterization and experimental design. (a) Optical image of bilayer (2L) black phosphorus (BP) sample (red outline). The circle represents the position of the laser beams on the sample for PL and μ-TAS experiment. (b) Schematic of the μ-TAS experiment on 2L BP. The energy band diagram shows the configuration of the pump and the probe energies used for the μ-TAS experiment. (c) Differential reflectivity plot with different probe wavelengths at the exciton resonance for 2L BP. (d) Comparison between the Stokes shifted PL and the pump-induced negative differential reflectivity at zero-time delay.

isolate the signal from just the bilayer region of the exfoliated flake. We recorded the differential reflectivity of the probe with and without the pump, from which one can also calculate the pump-induced transient absorption [25]. A schematic of our experiment is shown in Fig. 1(b), with further details in the Supplemental Material [20].

We plot the measured transient reflectivity for different probe wavelengths around the exciton resonance in Fig. 1(c) after exciting carriers just above the band gap with the pump pulse. We assume 5% absorption of the pump pulse [14], and that 60% of the created carriers form excitons within the first picosecond [26,27]. Similar to previous studies on TMDs, we assign the differential reflectivity at the exciton resonance to the presence of a pump-induced excitonic population [8,28]. Accordingly, we also observe the photoinduced bleach at the exciton resonance (blue) and photoinduced absorption (red) around it due to phase space filling effects [29]. The profile of the differential reflectivity at zero-time delay also matches well with the PL peak [Fig. 1(d)] with the expected slight Stokes shift to higher energies [14]. For subsequent experiments, we monitor the differential reflectivity of the probe wavelength at the maximum of the bleach signal (1.15 eV or 1070 nm) in the μ-TAS plots. We note that on photoexcitation, we observe a shift in the excitonic peak of around a few meV relative to the unphotoexcited excitonic absorption, determined by effects associated with the renormalization of the band gap and exciton binding energy [30]. To ensure that our measurement of exciton density is insensitive to such shifts, we integrate over a 10 meV bandwidth around the exciton peak energy. Moreover, our results and analysis remain unaltered when considering a 40 meV bandwidth, which is comparable to the exciton linewidth (see Supplemental Material, Fig. S5 [20]).

In order to investigate X-X annihilation, we vary our initial exciton density within the range from 5×10^{12} to 2.3×10^{13} cm^{-2}, where effects of X-X annihilation have previously been reported in atomically thin BP [31] and which is well above the defect density (see Supplemental Material, Sec. IV [20]). We exclude biexciton formation from our consideration, as we do not observe any additional peak in PL at high excitation power, nor in our TAS measurements. We focus on the system response only in the first few tens of picoseconds, where the annihilation process dominates. At these early timescales, we neglect contributions from the radiative recombination process which only dominate at longer timescales (hundreds of picoseconds) [29]. We also consider the role of electron-phonon interactions in understanding our observed carrier dynamics: Previous studies have reported that strong electron-phonon interactions contribute to the formation of excitons, and their rapid initial cooling on the sub- to few picosecond timescale [26,27,29,32]. Consistent with these reports, and with our 700 fs pulse duration, we see photobleaching at the excitonic resonance [Fig. 1(c)] even at zero delay. Thereafter, over the next few tens of picoseconds, electron-phonon interactions lead to a slower exchange of energy with the lattice, during which time X-X interactions dominate, and one can assume relatively constant lattice and electronic temperatures [29,32].

In Fig. 2(a), we plot the negative differential reflectivity $(-\Delta R/R)$, which is proportional to X_t, for high and low fluence. Compared to previous reports for isotropic semiconductors, we observe unusual behavior at early times; there is a faster decay for low excitation densities ($\sim 10^{12}$ cm^{-2}) versus high excitation densities. Furthermore, at later times, the decay for low excitation densities is slower compared to high excitation densities. This behavior at low intensities could be suggestive of 1D X-X annihilation processes, where time-dependent X-X scattering processes are initially fast, but then slow down at later times. Such 1D behavior may be reasonably expected in BP, due to its anisotropic nature. To explicitly understand the dimensional form of X-X annihilation, and to compare with previous literature, we plot our transient data as $(X_0/X_t) - 1$, where X_0, X_t are the exciton densities at time delay zero and t, respectively. For 1D systems, $(X_0/X_t) - 1$ is proportional to $\sqrt{t}$, as has been observed for CNTs [3,4] and 1D organic semiconductors [2,5,6], and $(X_0/X_t) - 1$ is proportional to t for 2D systems, as observed in 2D TMDs [8–10] (see Supplemental Material, Sec. X [20]).

We show the evolution of the dimensional form of X-X annihilation for atomically thin BP by plotting $(X_0/X_t) - 1$ versus time delay in Figs. 2(b)–2(d), for the range of initial exciton densities discussed above. At initial exciton

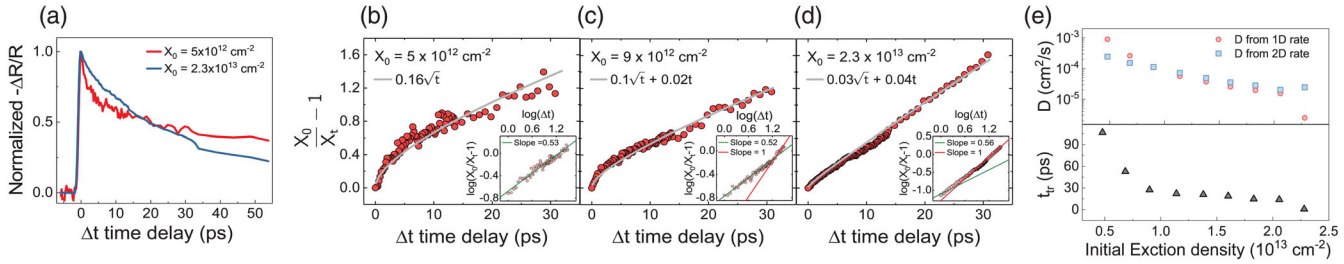

FIG. 2. 1D to 2D transformation of exciton-exciton annihilation in 2L BP. (a) Normalized $-\Delta R/R$ plot for different initial exciton density, (b)–(d) $(X_0/X_t) - 1$ versus time delay plotted for increasing initial exciton density (X_0) (left to right). The gray lines are $A\sqrt{t} + Bt$ fits to the data. The inset shows the $\log[(X_0/X_t) - 1]$ versus $\log(\Delta t)$ plot with the linear fits demonstrating the change in the slope from 0.5 to 1, corresponding to the transition from 1D to 2D. (e) Diffusion constants extracted from the 1D and 2D coefficients of the anisotropic diffusion limited X-X annihilation model and the transition time plotted versus initial exciton density.

densities of 10^{12} cm^{-2}, we observe the classic $\sqrt{t}$ behavior [Fig. 2(b)]. In BP, this 1D-like behavior is due to the strong anisotropy which results in the carriers diffusing rapidly along the armchair direction as compared to the zigzag direction. To first order, this larger diffusion constant along armchair results from the lower effective mass of carriers along the armchair direction [16,19]. Therefore, excitons largely interact with their nearest neighbors along the armchair direction, and thus exhibit the time-varying rates observed in 1D systems. Intrinsic anisotropy in the electron-phonon interaction can also contribute to the anisotropic mobility of carriers in few layer BP, although one expects this contribution to be weaker compared to the anisotropy in carrier effective masses [18]. In contrast, for initial exciton densities 10^{13} cm^{-2} [Fig. 2(d)], we see strikingly different behavior. $(X_0/X_t) - 1$ exhibits a linear dependence on time which is similar to the observed features in 2D systems like TMDs [9,10]. The linear time dependence represents X-X annihilation with a rate constant that is fixed in time, and a process that only depends on the local exciton densities.

To further understand this transition from 1D behavior to 2D behavior, we look more closely at intermediate exciton densities [Fig. 2(c)]. At early time delays, we see the 1D-like $\sqrt{t}$ behavior. Thereafter, the system evolves to display the characteristic 2D linear behavior, with a transition time (t_{tr}) that decreases with an increase in the initial exciton density. This is seen more clearly in a $\log[(X_0/X_t) - 1]$ versus $\log(t)$ plot [insets of Figs. 2(b)–2(d)] with the change in slope from ~0.5 to 1 denoting the transition from 1D to 2D behavior. For the lowest exciton density measured [Fig. 2(b)], the observed transition time falls out of the measured 30 ps and the data show a single 0.53 slope (green line) which corresponds to 1D behavior. At the highest density considered [Fig. 2(d)], the transition from a slope of ~0.56 to 1.0 occurs nearly within the time resolution of our system. In general, the data for all exciton density range can be fit to the form $(X_0/X_t) - 1 = A\sqrt{t} + Bt$, with the coefficients A and B varying with initial exciton density and representing the 1D and 2D rate coefficients (see Supplemental Material, Fig. S5 [20]). With this experimental observation, an intuitive picture of the phenomena can be obtained by recognizing that at a particular initial exciton density, the early time dynamics are dominated by a 1D interaction due to the preferred excitonic diffusion along the armchair direction. At later times, the slow diffusion along the zigzag direction causes excitons to start interacting in the second dimension, and the scattering begins to show 2D character. Although diffusion occurs simultaneously along the armchair and the zigzag direction, it takes longer time for the excitons to start interacting along the zigzag direction due to the low diffusion coefficient. Therefore, at later times, the scattering begins to show 2D character as the exciton can interact along both the armchair and the zigzag directions. With increasing initial exciton density, the mean distance between excitons decreases, causing a faster encounter between the excitons along the zigzag direction, and resulting in a faster transition into 2D-like scattering. A schematic of this intuitive explanation is depicted in Supplemental Material, Fig. S9 [20].

To quantitatively understand the observed behavior in BP, we applied the rate equation for X-X annihilation, $(dX/dt) = -kX^2$, using a diffusion-based model for two body scattering in anisotropic systems [33,34]. For such a system, the rate constant is given by

$$k = 2\pi D\left(\frac{\pi r_0}{2\sqrt{\pi D t}} + \frac{-4}{\ln(\pi r_0^2 X_0)}\right), \tag{1}$$

where $D = \sqrt{D_{ac}D_{zz}}$ is the geometric mean of the diffusion constants along the armchair and zigzag axes, r_0 is the annihilation radius, and X_0 is the initial exciton density. The first term in k occurs in 1D systems, and represents time-varying X-X scattering rates, whereas the second term is constant in time and is associated with the time-independent X-X scattering rates seen in 2D systems (see Supplemental Material, Sec. 11 [20]). In previous studies on anisotropic systems, both terms were needed to understand the observed phenomena. However, the effect of the

varying initial exciton density was not considered, as the experiments were performed at a fixed exciton density [33]. In our measurements on BP it is necessary to include the dependence on the initial exciton density in order to see a transition from 1D to 2D X-X annihilation.

Solving the bimolecular rate equation using the rate from Eq. (1), we get

$$\frac{X_0}{X_t} - 1 = 2\pi D X_0 \left(\frac{\pi r_0}{\sqrt{\pi D}} \sqrt{t} + \frac{-4}{\ln(\pi r_0^2 X_0)} t \right). \quad (2)$$

Comparing our numerical fits to the experimental data of the form $(X_0/X_t) - 1 = A\sqrt{t} + Bt$, one obtains $A = 2\pi^{3/2} r_0 \sqrt{D} X_0$ and $B = (-8\pi D X_0)/\ln(\pi r_0^2 X_0)$. Based on previous work on X-X annihilation in low-dimensional systems [35], we assume a radius of annihilation of 1 nm that is independent of the initial exciton density. This allows us to extract the diffusion constant for different initial exciton densities from both the A coefficient as well as the B coefficient. In Fig. 2(e) we plot this diffusion constant extracted from both these coefficients, which show consistent results. We note the decreasing trend of the diffusion constant with increasing exciton density, which is attributed to the predicted decrease in mobility of the carriers with increasing carrier densities in atomically thin BP [36]. The extracted diffusion coefficient of excitons is lower than previously reported for free carriers in BP [16], possibly due to lower mobility of excitons as well as the effects of the fused silica substrates [37–39]. Another important parameter which can be extracted from the experimental data is the transition time. It is defined as the time at which the 1D rate equals the 2D rate and is given by $t_{\mathrm{tr}} = (A/B)^2 = \{\pi r_0^2 [\ln(\pi r_0^2 X_0)]^2\}/16D$. As expected, the transition time is much slower for the relatively low exciton density range (10^{12} cm^{-2}) and becomes faster with increasing exciton density, as shown in Fig. 2(e).

The theoretical form of the X-X annihilation rate [Eq. (1)] immediately suggests another possibility to manipulate the relative strengths of the 1D rate to the 2D rate, given by $A/B = -[\sqrt{\pi} r_0 \ln(\pi r_0^2 X_0)]/4\sqrt{D}$. For a fixed diffusion constant, increasing the initial exciton density X_0 allows one to transition from 1D to 2D X-X annihilation. Now, at this fixed high initial exciton density, lowering the diffusion constant would recover 1D behavior [Fig. 3(a)]. To confirm this understanding, we lower the sample temperature as a means to lower the diffusion

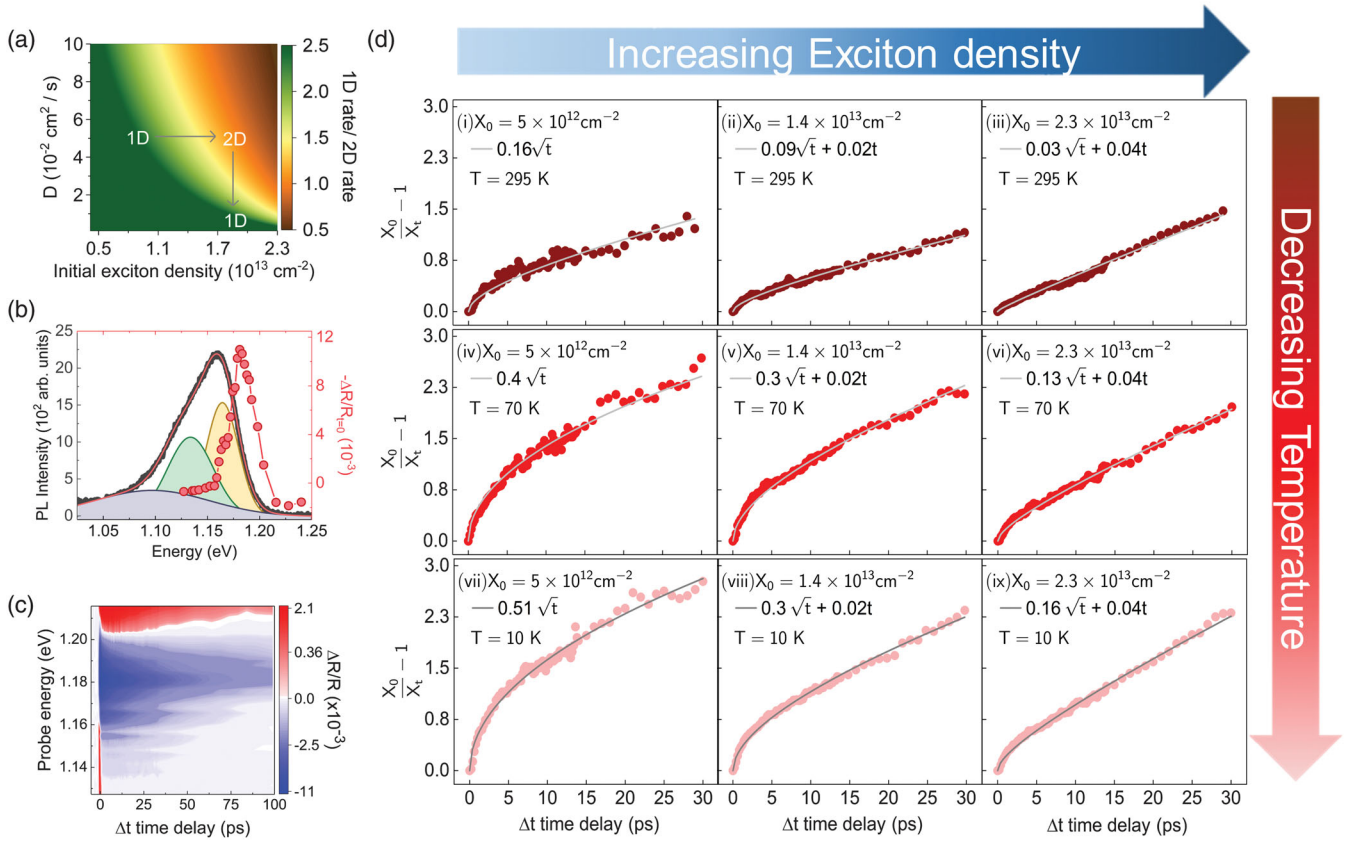

FIG. 3. Controlling the dimensionality of exciton-exciton annihilation with temperature and initial exciton density. (a) Theoretical plot of 1D rate/2D rate showing the dominant dimensional form versus diffusion constant and initial exciton density parameter space. (b) Stokes shifted PL from the $\Delta R/R$ at zero-time delay at 70 K showing mobile excitons, trions, and trapped exciton PL peaks. (c) $\Delta R/R$ plot for different probe wavelengths at exciton resonance for 2L BP sample at 70 K. (d) $(X_0/X_t) - 1$ versus time delay plotted for different temperatures and initial exciton densities.

constant [3,40] and perform corresponding PL and μ-TAS experiments. As previously observed in the case of 2D semiconductors, we see that the PL peak is blueshifted at low temperatures [41,42] and appears to be broadened due to the presence of additional peaks on the low energy side of the spectrum [Fig. 3(b)] [42]. These peaks have been identified as either trions or trapped excitons and show different dynamics than the mobile excitons [43,44]. Figure 3(c) shows the differential reflectivity plot for different probe energies at 70 K which shows multiple peaks, each with their own dynamics. The differential reflectivity spectrum at zero delay overlaid with the PL shows the expected Stokes shift for all peaks [Fig. 3(b)]. In particular, we see the prominent photoinduced bleach and photoinduced absorption features at and around the mobile exciton resonance, respectively. Accordingly, we carefully tune the probe energy to 1.18 eV (with a bandwidth of 10 meV) to match the peak response from mobile excitons. Similar to our room temperature analysis, in Fig. 3(d), we plot $(X_0/X_t) - 1$ versus time delay for decreasing temperature, as well as increasing initial exciton density. At high initial exciton densities [Figs. 3(d)(iii), 3(d)(vi), and 3(d)(ix)], we clearly see the recovery of $\sqrt{t}$ 1D behavior at early times for low temperatures [Fig. 3(d)(ix)] starting from the linear 2D behavior observed at room temperature [Fig. 3(d)(iii)].

In conclusion, we have shown the ability to fundamentally change the dimensional form of X-X annihilation in few layer BP by tuning the experimental parameters of temperature and initial exciton density. We can switch from the sublinear power-law decay seen in 1D systems to the standard linear decay observed in 2D systems in a single system. Given the operational limitations faced by devices due to X-X annihilation, particularly at high exciton densities, the understanding of this unique phenomenon in BP is important to fulfill its potential promise in optoelectronic applications. For example, it is well known that the high annihilation rates seen in 1D systems at early time delays prevent CNTs from exhibiting important phenomena, such as lasing [3] and the Mott-insulator transition [11], that are seen in 2D systems [12,13]. In BP, the transition to 2D X-X scattering at higher densities may allow one to achieve higher initial excitonic densities than naively expected assuming a quasi-1D system. From another perspective, to date, BP has drawn a lot of interest among the van der Waals family due to its quasi-1D nature. In this work, we have shown the ability to alter the dimensional form of a phenomenon beyond the known quasi-1D nature of BP by utilizing nonlinear interactions that play out in 2D. This adds an interesting twist to the potential versatility and utility of BP in optoelectronic functionality and as a unique platform to investigate dimensional changes in nonlinear phenomena.

The authors thank Bala Murali Krishna Mariserla and Andrew Winchester for helpful discussions. The authors also thank the Mechanical Engineering and Microfabrication Support Section of the Okinawa Institute of Science and Technology Graduate University for supporting characterization.

*kmdani@oist.jp

[1] T. Mueller and E. Malic, npj 2D Mater. Appl. **2**, 29 (2018).
[2] V. Gulbinas, M. Chachisvilis, L. Valkunas, and V. Sundstrom, J. Phys. Chem. **100**, 2213 (1996).
[3] A. Srivastava and J. Kono, Phys. Rev. B **79**, 205407 (2009).
[4] M. W. Graham, Y.-Z. Ma, A. A. Green, M. C. Hersam, and G. R. Fleming, in *Ultrafast Phenomena in Semiconductors and Nanostructure Materials XIV*, International Society for Optics and Photonics Vol. 7600, edited by J.-J. Song, K.-T. Tsen, M. Betz, and A. Y. Elezzabi (SPIE-International Society for Optical Engineering, Bellingham, WA, 2010), pp. 282–294, https://doi.org/10.1117/12.841194.
[5] E. Engel, K. Leo, and M. Hoffmann, Chem. Phys. **325**, 170 (2006).
[6] Y. Z. Ma, K. Xiao, and R. W. Shaw, J. Phys. Chem. C **116**, 21588 (2012).
[7] P. L. Krapivsky, S. Redner, and E. Ben-Naim, *A Kinetic View of Statistical Physics* (Cambridge University Press, Cambridge, England, 2010).
[8] D. Sun, Y. Rao, G. A. Reider, G. Chen, Y. You, L. Brézin, A. R. Harutyunyan, and T. F. Heinz, Nano Lett. **14**, 5625 (2014).
[9] Y. Yu, Y. Yu, C. Xu, A. Barrette, K. Gundogdu, and L. Cao, Phys. Rev. B **93**, 201111(R) (2016).
[10] N. Kumar, Q. Cui, F. Ceballos, D. He, Y. Wang, and H. Zhao, Phys. Rev. B **89**, 125427 (2014).
[11] Y. Murakami and J. Kono, Phys. Rev. Lett. **102**, 037401 (2009).
[12] Y. Ye, Z. J. Wong, X. Lu, X. Ni, H. Zhu, X. Chen, Y. Wang, and X. Zhang, Nat. Photonics **9**, 733 (2015).
[13] A. Chernikov, C. Ruppert, H. M. Hill, A. F. Rigosi, and T. F. Heinz, Nat. Photonics **9**, 466 (2015).
[14] L. Li, J. Kim, C. Jin, G. J. Ye, D. Y. Qiu, F. H. Da Jornada, Z. Shi, L. Chen, Z. Zhang, F. Yang, K. Watanabe, T. Taniguchi, W. Ren, S. G. Louie, X. H. Chen, Y. Zhang, and F. Wang, Nat. Nanotechnol. **12**, 21 (2017).
[15] S. Zhang, J. Yang, R. Xu, F. Wang, W. Li, M. Ghufran, Y.-W. Zhang, Z. Yu, G. Zhang, Q. Qin, and Y. Lu, ACS Nano **8**, 9590 (2014).
[16] J. He, D. He, Y. Wang, Q. Cui, M. Z. Bellus, H. Y. Chiu, and H. Zhao, ACS Nano **9**, 6436 (2015).
[17] V. Tran, R. Fei, and L. Yang, 2D Mater. **2**, 044014 (2015).
[18] J. Qiao, X. Kong, Z. X. Hu, F. Yang, and W. Ji, Nat. Commun. **5**, 4475 (2014).
[19] B. Liao, H. Zhao, E. Najafi, X. Yan, H. Tian, J. Tice, A. J. Minnich, H. Wang, and A. H. Zewail, Nano Lett. **17**, 3675 (2017).
[20] See Supplemental Material http://link.aps.org/supplemental/10.1103/PhysRevLett.124.057403 for brief discussion on experimental setup, power dependent PL, which includes Refs. [21,22], analysis with larger probe bandwidth, derivation of the dynamical form of 1D and 2D interactions, schematic understanding of 1D-2D transition in 2L BP, and derivation of the anisotropic diffusion limited rate.

[21] S. Draguta, S. Thakur, Y. V. Morozov, Y. Wang, J. S. Manser, P. V. Kamat, and M. Kuno, J. Phys. Chem. Lett. **7**, 715 (2016).
[22] F. Vietmeyer, P. A. Frantsuzov, B. Janko, and M. Kuno, Phys. Rev. B **83**, 115319 (2011).
[23] A. Carvalho, M. Wang, X. Zhu, A. S. Rodin, H. Su, and A. H. C. Neto, Nat. Rev. Mater. **1**, 16061 (2016).
[24] V. Tran, R. Soklaski, Y. Liang, and L. Yang, Phys. Rev. B **89**, 235319 (2014).
[25] E. J. Sie, Time-resolved absorption spectroscopy, in *Coherent Light-Matter Interactions in Monolayer Transition-Metal Dichalcogenides* (Springer International Publishing, Cham, 2018), pp. 13–25.
[26] P. Steinleitner, P. Merkl, P. Nagler, J. Mornhinweg, C. Schüller, T. Korn, A. Chernikov, and R. Huber, Nano Lett. **17**, 1455 (2017).
[27] Z. Nie, R. Long, L. Sun, C.-C. Huang, J. Zhang, Q. Xiong, D. W. Hewak, Z. Shen, O. V. Prezhdo, and Z.-H. Loh, ACS Nano **8**, 10931 (2014).
[28] F. Ceballos and H. Zhao, Adv. Funct. Mater. **27**, 1604509 (2017).
[29] C. Ruppert, A. Chernikov, H. M. Hill, A. F. Rigosi, and T. F. Heinz, Nano Lett. **17**, 644 (2017).
[30] X. Miao, G. Zhang, F. Wang, H. Yan, and M. Ji, Nano Lett. **18**, 3053 (2018).
[31] A. Surrente, A. A. Mitioglu, K. Galkowski, L. Klopotowski, W. Tabis, B. Vignolle, D. K. Maude, and P. Plochocka, Phys. Rev. B **94**, 075425 (2016).
[32] C. Robert, D. Lagarde, F. Cadiz, G. Wang, B. Lassagne, T. Amand, A. Balocchi, P. Renucci, S. Tongay, B. Urbaszek, and X. Marie, Phys. Rev. B **93**, 205423 (2016).
[33] U. Gösele and A. Seeger, Philos. Mag. **34**, 177 (1976).
[34] C. Woo, in *Proceedings of the 13th International Symposium on Radiation-Induced Changes in Microstructure (Part I)* (ASTM International, 1987), pp. 70–89, https://doi.org/10.1520/STP33809S.
[35] P. E. Shaw, A. Ruseckas, and I. D. W. Samuel, Adv. Mater. **20**, 3516 (2008).
[36] Y. Trushkov and V. Perebeinos, Phys. Rev. B **95**, 075436 (2017).
[37] B. Radisavljevic, A. Radenovic, J. Brivio, V. Giacometti, and A. Kis, Nat. Nanotechnol. **6**, 147 (2011).
[38] B. Radisavljevic and A. Kis, Nat. Mater. **12**, 815 (2013).
[39] K. S. Novoselov, D. Jiang, F. Schedin, T. J. Booth, V. V. Khotkevich, S. V. Morozov, and A. K. Geim, Proc. Natl. Acad. Sci. U.S.A. **102**, 10451 (2005).
[40] O. V. Mikhnenko, F. Cordella, A. B. Sieval, J. C. Hummelen, P. W. Blom, and M. A. Loi, J. Phys. Chem. B **112**, 11601 (2008).
[41] T. Korn, S. Heydrich, M. Hirmer, J. Schmutzler, and C. Schller, Appl. Phys. Lett. **99**, 102109 (2011).
[42] J. Yang, R. Xu, J. Pei, Y. W. Myint, F. Wang, Z. Wang, S. Zhang, Z. Yu, and Y. Lu, Light Sci. Appl. **4**, e312 (2015).
[43] T. Godde, D. Schmidt, J. Schmutzler, M. Aßmann, J. Debus, F. Withers, E. M. Alexeev, O. Del Pozo-Zamudio, O. V. Skrypka, K. S. Novoselov, M. Bayer, and A. I. Tartakovskii, Phys. Rev. B **94**, 165301 (2016).
[44] A. Singh, G. Moody, K. Tran, M. E. Scott, V. Overbeck, G. Berghäuser, J. Schaibley, E. J. Seifert, D. Pleskot, N. M. Gabor, J. Yan, D. G. Mandrus, M. Richter, E. Malic, X. Xu, and X. Li, Phys. Rev. B **93**, 041401(R) (2016).